Analytical cumulant solution of the vector radiative transfer equation investigates backscattering of circularly polarized light from turbid media

Wei Cai, Xiaohui Ni, S. K. Gayen, and R. R. Alfano
Institute for Ultrafast Spectroscopy and Lasers, Department of Physics, The City College of City University of New York, New York, New York 10031, USA
(Received 6 April 2006; published 8 November 2006)

The backscattering of circularly polarized light pulses from an infinite uniform scattering medium is studied as a function of helicity of the incident light and size of scatterers in the medium. The approach considers a polarized short pulse of light incident on the scattering medium, and uses an analytical cumulant solution of the vector radiative transfer equation with the phase matrix obtained from the Mie theory to calculate the temporal profile of scattered polarized photons for any position and any angle of detection. The general expression for the scattered photon distribution function is an expansion in spatial cumulants up to an arbitrary high order. Truncating the expansion at the second-order cumulant, a Gaussian analytical approximate expression for the temporal profile of scattered polarized photons is obtained, whose average center position and half width are always exact. The components of scattered light copolarized and cross polarized with that of the incident light can be calculated and used for determining the degree of polarization of the scattered light. The results show that circularly polarized light of the same helicity dominates the backscattered signal when scatterer size is larger than the wavelength of light. For the scatterers smaller than the wavelength, the light of opposite helicity makes the dominant contribution to the backscattered signal. The theoretical estimates are in good agreement with our experimental results.

DOI: 10.1103/PhysRevE.74.056605 PACS number(s): 42.25.Dd, 42.25.Ja, 42.68.Ay

I. INTRODUCTION

The recent increased interest in the study [1–12] of polarized light propagation through turbid media derives from a variety of practical applications. Polarized light multiple scattered from a turbid medium carries information about the medium interior [13] such as, particle size and concentration, size distribution, and refractive index variation, which can be useful for biomedical imaging [13–15], endoscopic evaluation of biological tissues [16], investigation of biological cell differentiation [17,18], flow cytometry [18,19], lidar-based remote sensing of the atmospheric cloud, aerosol fog and smog [20,21], and imaging of targets in shallow coastal water [22]. Polarization-sensitive imaging has been demonstrated to enhance image contrast of targets embedded in turbid media [14,23].

In particular, it has been observed that for circularly polarized light, randomization of its polarization requires more scattering events than the randomization of its direction [23–27,6,9]. An important consequence of this "polarization memory" [25] is higher resolution and contrast of transillumination images recorded with copolarized light than those recorded with unpolarized or cross-polarized light. Another interesting feature is the dependence of the intensity of the backscattered copolarized and cross-polarized light on the size of the scatterers in the medium [23]. The backscattered light is dominated by light of helicity opposite to that of the incident light if the size of the scatterers is smaller than the wavelength of light. The light of the same helicity dominates when scatterers are larger than the light wavelength. These results have important consequences in the design considerations of imaging systems using backscattered light such as, endoscopic systems. All these developments make it imperative that theoretical formalisms be developed to provide a quantitative explanation of the experimental results, and guidance for the design of imaging systems using polarized light.

Theoretical studies of polarized light propagation through a scattering medium commonly starts with the vector radiative transfer equation (VRTE) [1], and because of the inherent complexity of the problem, a limited number of studies are available to date. A majority of these studies focused on developing numerical solutions of the VRTE. Ishimaru and co-workers first investigated the propagation of continuous wave (CW), polarized wave normally incident on a medium with discrete scatterers using discrete ordinate methods to solve VRTE [2,3]. More recently, they extended the formalism to numerically solve the time-dependent VRTE to account for the propagation of polarized pulses [4]. Kim and Moscoso studied the propagation of a linearly polarized or circularly polarized continuous plane wave normally incident on a plane-parallel medium containing a random distribution of dielectric spheres, and numerically solved the one-dimensional VRTE using a Chebyshev spectral method [5]. The approach was subsequently modified to study the backscattering of circularly polarized plane-wave pulses [6]. Vallion *et al.* [7] used a vector Monte Carlo method to study polarized light transport through a semitransparent medium filled with scattering particles. Jiang *et al.* [8] developed a multilayer radiative transfer model that takes into account the state of polarization using the doubling-adding method for passive atmospheric remote sensing applications. More recently, Sakami and Dogariu [9] investigated the propagation of a polarized plane-wave pulse incident at any angle in a random medium using the discrete-ordinates method to

solve the VRTE, and used an angular analysis to obtain details of the polarization flip of circular polarized light. The problem of light scattering and radiative transfer in scattering media and its application to geophysical optics, image transfer, remote sensing, and inverse problems are discussed in the monograph by Kokhanovsky [10].

In this paper, we use the analytical solution of the time-dependent VRTE to compute backscattering of circularly polarized light in an infinite uniform scattering medium. It builds on the analytical cumulant approach for solving the time-dependent radiative transfer equation in an infinite uniform medium that we developed [28–30]. In this approach an arbitrary phase function, as long as it is a function of scattering angle, can be treated. We have derived the exact expression of spatial cumulants of photon distribution at any angle and any time, up to an arbitrary high order. The exact first spatial cumulant represents the center of the distribution and the exact second spatial cumulant represents the width of the distribution. The method of the analytical cumulant solution for the scalar radiative transfer equation can be extended to the vector (polarized) case [31]. In the analytical solution of VRTE, a transform to the circular representation from the Stokes representation of polarization is introduced, and the generalized spherical functions are used for angular expansion, instead of the standard spherical functions for solving the scalar radiative transfer equation. The expressions for the exact first and second spatial cumulants of polarized components as functions of angle $\mathbf{s}$ and time t is derived. Then, intensity of the polarized light is presented by a Gaussian spatial distribution. We apply this method to calculate the backscattering of circular polarized light in a scattering medium. The results show that circularly polarized light of the same helicity dominates the backscattered signal when scatterer size is larger than the wavelength of light. For the scatterers smaller than the wavelength, light of opposite helicity makes the dominant contribution to the backscattered signal. The theoretical conclusion is in good agreement with our experimental results [23].

The paper is organized as follows. In Sec. II we review the analytical solution of VRTE. In Sec. III, the numerical results are presented and are compared with experiments. Section IV is devoted to discussion and conclusion.

II. THEORETICAL FORMALISM

A. Polarized components of light

In the Stokes polarization representation [32] (SP), the polarized light is described by $\mathbf{I}^{SP}=[I,Q,U,V]$. The polarized components of distribution we will study are the parallel component $I_{\|}=(I+Q)/2$, the perpendicular component $I_{\perp}=(I-Q)/2$, the right-circular component $I_R=(I+V)/2$, and the left-circular component $I_L=(I-V)/2$, since these quantities are positive definite, and are experimentally measurable.

The vector radiative transfer equation for the polarized photon distribution function $\mathbf{I}(\mathbf{r},\mathbf{s},t)$ in an infinite uniform medium, illuminated by a point light source providing short pulse, $\mathbf{I}^{(0)}\delta(\mathbf{r}-\mathbf{r}_0)\delta(\mathbf{s}-\mathbf{s}_0)\delta(t-0)$ is given by [33]

$$\partial\mathbf{I}(\mathbf{r},\mathbf{s},t)/\partial t + c\mathbf{s}\cdot\nabla_{\mathbf{r}}\mathbf{I}(\mathbf{r},\mathbf{s},t) + \mu_a\mathbf{I}(\mathbf{r},\mathbf{s},t) = \mu_s\int \mathbf{P}(\mathbf{s},\mathbf{s}')[\mathbf{I}(\mathbf{r},\mathbf{s}',t)-\mathbf{I}(\mathbf{r},\mathbf{s},t)]d\mathbf{s}' + \mathbf{I}^{(0)}\delta(\mathbf{r}-\mathbf{r}_0)\delta(\mathbf{s}-\mathbf{s}_0)\delta(t-0), \quad (1)$$

where vector $\mathbf{I}(\mathbf{r},\mathbf{s},t)$ has four polarization components, c is the light speed in the medium, μ_s is the scattering rate, μ_a is the absorption rate, and $\mathbf{P}(\mathbf{s},\mathbf{s}')$ is the 4×4 phase matrix. A meridian plane parallel to the z axis and the light direction $\mathbf{s}$, is used as a plane of reference for the description of the polarization state. In SP the components Q,U vary with the rotation of the reference plane around the light propagation direction. With a rotation of reference plane through an angle $\alpha\geqslant0$ (in the counterclockwise direction, when looking in the direction of propagation) $\mathbf{I}^{SP}$ varies as $(\mathbf{I}')^{SP}=\mathbf{L}(\alpha)\mathbf{I}^{SP}$, where $\mathbf{L}(\alpha)$ is given by

$$\mathbf{L}(\alpha)=\begin{bmatrix}1 & 0 & 0 & 0\\ 0 & \cos2\alpha & \sin2\alpha & 0\\ 0 & -\sin2\alpha & \cos2\alpha & 0\\ 0 & 0 & 0 & 1\end{bmatrix}. \quad (2)$$

When light propagates along the z direction, Q,U vary with the change of the azimuthal angle ϕ.

The phase matrix in the fixed coordinates is given by:

$$\mathbf{P}(\mathbf{s},\mathbf{s}')=\mathbf{L}(\pi-\chi)\mathbf{P}(\cos\Theta)\mathbf{L}(-\chi'), \quad (3)$$

where Θ is the angle between light rays before and after scattering in the scattering plane, and the matrices $\mathbf{L}(-\chi')$ and $\mathbf{L}(\pi-\chi)$ are those required to rotate meridian planes before and after scattering onto a local scattering plane. The intrinsic property of a scattering mechanism is described by the 4×4 scattering function $\mathbf{P}(\cos\Theta)$, which is assumed to depend only on $\cos\Theta=\mathbf{s}\cdot\mathbf{s}'$. It is convenient to use a representation of the polarized light in which $\mathbf{L}(\alpha)$ is diagonal, rather than Eq. (2). A circular polarization representation (CP), first proposed by Kuščer and Ribarič [34] and presented by Hovenier and van der Mee [35], is $I^{CP}=[I_2,I_0,I_{-0},I_{-2}]$, where $I_0=(I+V)/2$, $I_{-0}=(I-V)/2$, $I_2=(Q+iU)/2$, and $I_{-2}=(Q-iU)/2$, or $\mathbf{I}^{CP}=\mathbf{T}\mathbf{I}^{SP}$, with

$$\mathbf{T}=\frac{1}{2}\begin{bmatrix}0 & 1 & i & 0\\ 1 & 0 & 0 & 1\\ 1 & 0 & 0 & -1\\ 0 & 1 & -i & 0\end{bmatrix} \text{ and } \mathbf{T}^{-1}=\begin{bmatrix}0 & 1 & 1 & 0\\ 1 & 0 & 0 & 1\\ -i & 0 & 0 & i\\ 0 & 1 & -1 & 0\end{bmatrix}. \quad (4)$$

In CP a rotation of the reference plane through an angle α around the light direction causes I_m^{CP} to be multiplied by $\exp(-im\alpha)$, $m=2,0,0,-2$. Notice that I_0 and I_{-0} actually have the same rotational property. For the phase matrix, transform between two representations is $\mathbf{P}^{CP}=\mathbf{T}\mathbf{P}^{SP}\mathbf{T}^{-1}$.

In CP it is convenient to expand the phase matrix $\mathbf{P}^{CP}$ using the generalized spherical functions (GSF). The generalized spherical functions $P^l_{mn}(\beta)$ are related to the $d^l_{mn}(\beta)$

in the angular momentum theory [36] by $P^l_{m,n}(\beta) = (i)^{m-n} d^l_{mn}(\beta)$. In the Appendix, the expressions for $d^l_{mn}(\beta)$ are presented.

B. Phase matrix using Mie theory

Elements of the CP phase matrix in the scattering plane, $P^{CP}_{mn}(\cos\Theta)$ can be expanded by GSF;

$$P^{CP}_{mn}(\cos\Theta) = \frac{1}{4\pi}\sum_l \rho^l_{mn} P^l_{m,n}(\cos\Theta), \tag{5}$$

with $m,n=2,0,-0,-2$, and $l \geqslant \max(|m|,|n|)$. The coefficients ρ^l_{mn} provide a description of the scattering mechanism. In most useful cases, the coefficients ρ^l_{mn} have properties: (i) $\rho^l_{mm}=\rho^l_{m-m}$ are real; (ii) $\rho^l_{mn}=\rho^l_{nm}=\rho^l_{-m-n}$; (iii) $\rho^l_{20}=[\rho^l_{2-0}]^*$ (* means complex conjugate). Therefore, for each $l \geqslant 2$, there are six independent real elements: ρ^l_{00}, ρ^l_{22}, ρ^l_{0-0}, ρ^l_{2-2}, $\mathrm{Re}[\rho^l_{20}]$, and $\mathrm{Im}[\rho^l_{20}]$. For $l=0,1$, only ρ^l_{00} and ρ^l_{0-0} are nonzero. These numerical coefficients can be calculated using the Mie theory for a spherical particle. We have $\rho^l_{00}=(\alpha^l_1+\alpha^l_4)/2$, $\rho^l_{0-0}=(\alpha^l_1-\alpha^l_4)/2$, $\rho^l_{22}=(\alpha^l_2+\alpha^l_3)/2$, $\rho^l_{2-2}=(\alpha^l_2-\alpha^l_3)/2$, $\mathrm{Re}[\rho^l_{20}]=\beta^l_1$, $\mathrm{Im}[\rho^l_{20}]=\beta^l_2$, where the coefficients $\alpha^l_{1,2,3,4}$ and $\beta^l_{1,2}$ are formulated in Eqs. (4.81)–(4.86) in Ref. [37].

C. Photon angular distribution $\mathbf{F}(\mathbf{s},\mathbf{s}_0,t)$

When we make a spherical harmonics expansion of Eq. (1), the difficulty is that the term $c\mathbf{s}\cdot\nabla_{\mathbf{r}}\mathbf{I}(\mathbf{r},\mathbf{s},t)$ couples equations of different harmonics. We first study the photon distribution in the angular space in CP initially incident along $\mathbf{s}_0$,

$$\mathbf{F}(\mathbf{s},\mathbf{s}_0,t) = \int \mathbf{I}(\mathbf{r},\mathbf{s},t)d\mathbf{r}, \tag{6}$$

where integration is over the whole space. Evaluation of the integral in Eq. (6) over Eq. (1) leads to

$$\begin{aligned}&\partial\mathbf{F}(\mathbf{s},\mathbf{s}_0,t)/\partial t + \mu_a\mathbf{F}(\mathbf{s},\mathbf{s}_0,t)\\ &\quad + \mu_s\left[\mathbf{F}(\mathbf{s},\mathbf{s}_0,t) - \int \mathbf{P}(\mathbf{s},\mathbf{s}')\mathbf{F}(\mathbf{s}',\mathbf{s}_0,t)d\mathbf{s}'\right]\\ &\quad = \mathbf{I}^{(0)}\delta(\mathbf{s}-\mathbf{s}_0)\delta(t-0).\end{aligned} \tag{7}$$

The gradient term disappears in Eq. (7) because of the Gauss-Stokes law. Hence, $\mathbf{F}(\mathbf{s},\mathbf{s}_0,t)$ can be exactly solved by expanding in GSF's. When $\mathbf{s}_0$ is set along the z direction, the initial polarization state is set as n_0, and the initial reference plane is set as the x-z plane, we have

$$\begin{aligned}F_{mn_0}(\mathbf{s},\mathbf{s}_0,t) = \sum_l \Bigg[&F^l_{mn_0}(t)P^l_{m,n_0}(\cos\theta)\\ &- \delta_{m,n_0}\frac{2l+1}{4\pi}e^{-\mu_s t}P^l_{0,0}(\cos\theta)\Bigg]\\ &\times\exp(-in_0\phi)\exp(-\mu_a t),\end{aligned} \tag{8}$$

where $\mathbf{s}=(\theta,\phi)$, and $m,n_0=2,0,-0,-2$, $l \geqslant \max(|m|,|n_0|)$. The second term in Eq. (8) represents the ballistic (unscattered) component of photons. $F^l_{mn_0}(t)$ in Eq. (8) is the solution of the equation

$$dF^l_{mn_0}(t)/dt = \sum_n \Pi^l_{mn}F^l_{nn_0}(t), \tag{9}$$

under the initial condition

$$F^l_{mn_0}(t=0) = \delta_{m,n_0}(2l+1)/4\pi, \tag{10}$$

where $\Pi^l_{mn}=\mu_s[\delta_{m,n}-\rho^l_{mn}/(2l+1)]$. The solution $F^l_{mn_0}(t)$ has the following form:

$$F^l_{mn_0}(t) = \frac{2l+1}{4\pi}\sum_i [B^l_{mn_0}]_i \exp(-\lambda^l_i t), \tag{11}$$

$i=1,2,3,4$ for $l \geqslant 2$, and $i=1,2$ for $l=1,2$. The eigenvalues λ^l_i for $l \geqslant 2$ is given by

$$\begin{aligned}\lambda^l_i = (1/2)\Bigg\{&(\Pi^l_{00}+\Pi^l_{22} \pm \Pi^l_{0-0} \pm \Pi^l_{2-2})\\ &+ \Bigg[(\Pi^l_{00}-\Pi^l_{22} \pm \Pi^l_{0-0} \mp \Pi^l_{2-2})^2\\ &\pm 16\begin{pmatrix}\mathrm{Re}[\Pi^l_{20}]\\ \mathrm{Im}[\Pi^l_{20}]\end{pmatrix}^2\Bigg]^{1/2}\Bigg\},\end{aligned} \tag{12}$$

for $i=1,2$, and for $i=3,4$, the sign $+$ before the square brackets in Eq. (12) is replaced by $-$. For $l=0,1$ two eigenvalues are $\lambda^l_i=\Pi^l_{00}\pm\Pi^l_{0-0}$. The constant coefficients $[B^l_{mn_0}]_i$ can be determined using linear algebra under the initial condition Eq. (10) [31].

In SP the angular distribution component of $I_m=[I,Q,U,V]$, with the initial polarized state $\mathbf{I}^{SP(0)}$, is obtained by

$$F^{SP}_m(\mathbf{s},\mathbf{s}_0,t) = [\mathbf{T}^{-1}\mathbf{F}(\mathbf{s},\mathbf{s}_0,t)\mathbf{T}\mathbf{I}^{SP(0)}]_m. \tag{13}$$

The angular distribution for the parallel polarized component is given by $F_\parallel(\mathbf{s},\mathbf{s}_0,t)=[F^{SP}_I(\mathbf{s},\mathbf{s}_0,t)+F^{SP}_Q(\mathbf{s},\mathbf{s}_0,t)]/2$. Similarly, we have $F_\perp=(F^{SP}_I-F^{SP}_Q)/2$, $F_R=(F^{SP}_I+F^{SP}_V)/2$, and $F_L=(F^{SP}_I-F^{SP}_V)/2$.

D. The cumulant expansion

The polarized photon distribution $I_m(\mathbf{r},\mathbf{s},t)$ in an infinite uniform medium can be written as [31]

$$I_m(\mathbf{r},\mathbf{s},t) = \left\langle \delta\left(\mathbf{r}-c\int_0^t \mathbf{s}(t')dt'\right)\delta[\mathbf{s}(t)-\mathbf{s}]\right\rangle_m, \tag{14}$$

where $\langle\cdots\rangle$ means the ensemble average in the angular space. We perform a Fourier transform of the first δ function, then make a cumulant expansion, and obtain

$$I_m(\mathbf{r},\mathbf{s},t) = F_m(\mathbf{s},\mathbf{s}_0,t)\frac{1}{(2\pi)^3}\int d\mathbf{q}\,\exp\Bigg\{ i\mathbf{q}\cdot\mathbf{r} + \sum_{k=1}^{\infty}\frac{(-ic)^k}{k!}\sum_{j_k}\cdots\sum_{j_1} q_{j_k}\cdots q_{j_1} \times\left[\left\langle\int_0^t dt_k\cdots\int_0^t dt_1 T[s_{j_k}(t_k)\cdots s_{j_1}(t_1)]\right\rangle_c\right]_m\Bigg\}, \tag{15}$$

where T denotes time-ordered multiplication [38], and the subscript-index c denotes cumulant. The cumulants are related to the moments. For an arbitrary random variable A, we have $\langle A\rangle_c=\langle A\rangle$, $\langle A^2\rangle_c=\langle A^2\rangle-\langle A\rangle\langle A\rangle$, and so on. The corresponding moment can be estimated using a standard time-dependent Green's-function approach, which is given by

$$\begin{aligned}\left[\left\langle\int_0^t dt_k\cdots\int_0^t dt_1 T[s_{j_k}(t_k)\cdots s_{j_1}(t_1)]\right\rangle\right]_m &= \frac{1}{F_m(\mathbf{s},\mathbf{s}_0,t)}\Bigg\{\Bigg[\int_0^t dt_k\int_0^{t_k} dt_{k-1}\cdots\int_0^{t_2} dt_1\int d\mathbf{s}^{(k)} \times\int d\mathbf{s}^{(k-1)}\cdots\int d\mathbf{s}^{(1)}\mathbf{F}(\mathbf{s},\mathbf{s}^{(k)},t-t_k)s_{j_k}^{(k)} \times\mathbf{F}(\mathbf{s}^{(k)},\mathbf{s}^{(k-1)},t_k-t_{k-1})s_{j_{k-1}}^{(k-1)}\cdots\mathbf{F}(\mathbf{s}^{(2)},\mathbf{s}^{(1)},t_2-t_1)s_{j_1}^{(1)} \times\mathbf{F}(\mathbf{s}^{(1)},\mathbf{s}_0,t_1-0)\mathbf{I}^{(0)}\Bigg]_m + (\text{perm})\Bigg\},\end{aligned} \tag{16}$$

where the abbreviation "perm" means all $k!-1$ terms obtained by permutation of $\{j_i\}$, $i=1,\ldots,k$ from the first term, and $\mathbf{F}(\mathbf{s}^{(i)},\mathbf{s}^{(i-1)},t_i-t_{i-1})$ is the exact solution given by Eq. (8) in Sec. II C. If we cut off the summation in Eq. (15) at $k=2$, the integration leads to a Gaussian spatial distribution characterized by the first and second cumulants.

1. First cumulant (center of the spatial distribution)

In CP it is convenient to set $\mathbf{s}$ in a spherical harmonic basis,

$$\mathbf{s}=[s_1,s_0,s_{-1}]=[-2^{-1/2}\sin\theta e^{+i\phi},\cos\theta,+2^{-1/2}\sin\theta e^{-i\phi}], \tag{17}$$

which is related to Cartesian component basis $\alpha=x,y,z$ by $s_\alpha=\Sigma U_{\alpha j}s_j$, $j=1,0,-1$ with

$$U=2^{-1/2}\begin{bmatrix}-1 & 0 & 1\\ i & 0 & i\\ 0 & 2^{1/2} & 0\end{bmatrix}. \tag{18}$$

Using the recurrence relation and the orthogonality relation of GSF, the unnormalized first moment in CP, when $\mathbf{s}_0$ is along the z direction, is obtained;

$$\begin{aligned}\langle\mathbf{R}_j\rangle_{mn_0} &= c\int_0^t dt'\int d\mathbf{s}'\sum_n F_{mn}(\mathbf{s},\mathbf{s}',t-t')s_j'F_{nn_0}(\mathbf{s}',\mathbf{s}_0,t') \\ &= c\sum_l\Bigg\{P^l_{m,n_0-j}(\cos\theta)e^{-i(n_0-j)\phi}\gamma_j\sum_n\sum_h\frac{2(l-h)+1}{4\pi} \times D^{l,h}_{m,n,n_0}(t)\langle l-h,1,n,0|l,n\rangle\langle l-h,1,n_0,-j|l,n_0-j\rangle \\ &\quad -\delta_{j,0}\delta_{m,n_0}\frac{2l+1}{4\pi}te^{-\mu_s t}P^l_{0,0}(\cos\theta)e^{-in_0\phi}\Bigg\},\end{aligned} \tag{19}$$

with $\gamma_{\pm1}=\mp i$, $\gamma_0=1$, $\langle l_1,l_2,m_1,m_2|L,M\rangle$ is Clebsch-Gordan coefficients in angular momentum theory [36], presented in the Appendix, and

$$D^{l,h}_{m,n,n_0}(t) = \sum_{i,j}[B^l_{mn}]_i[B^{l-h}_{nn_0}]_j\left(\frac{\exp(-\lambda_j^{l-h}t)-\exp(-\lambda_i^l t)}{\lambda_i^l-\lambda_j^{l-h}}\right) \times\exp(-\mu_a t), \tag{20}$$

where $i,j=1,2,3,4$ for $l\geqslant 2$, and $i,j=1,2$ for $l=1,2$.

In SP the component of the unnormalized first moment of $I_m=[I,Q,U,V]$, with the initial polarized state $\mathbf{I}^{SP(0)}$, and $\alpha=x,y,z$, is obtained by

$$\langle\mathbf{R}_\alpha\rangle_m^{SP} = \sum_j U_{\alpha j}[\mathbf{T}^{-1}\langle\mathbf{R}_j\rangle\mathbf{T}\mathbf{I}^{SP(0)}]_m. \tag{21}$$

The center of photon distribution for the linearly polarized components is obtained by

$$R^c_{p,\alpha}(\mathbf{s},t) = \frac{[\langle\mathbf{R}_\alpha\rangle_I^{SP}\pm\langle\mathbf{R}_\alpha\rangle_Q^{SP}]}{2F_p(\mathbf{s},\mathbf{s}_0,t)}, \tag{22}$$

where the + sign holds for the $p=\parallel$ component, and the − sign holds for the $p=\perp$ component. The center of photon distribution for the circularly polarized components is obtained by

$$R^c_{c,\alpha}(\mathbf{s},t) = \frac{[\langle\mathbf{R}_\alpha\rangle_I^{SP}\pm\langle\mathbf{R}_\alpha\rangle_V^{SP}]}{2F_c(\mathbf{s},\mathbf{s}_0,t)}, \tag{23}$$

where the + sign holds for the $c=R$ component, and the − sign holds for the $c=L$ component.

2. Second cumulant (width of the spatial distribution)

Similarly, we can obtain the expression for the unnormalized second moment in CP,

$$\langle \mathbf{R}_{j_2}\mathbf{R}_{j_1}\rangle_{mn_0} = c^2 \sum_l \left\{ P^l_{m,n_0-j_1-j_2}(\cos\theta) e^{-i(n_0-j_1-j_2)\phi} \gamma_{j_2}\gamma_{j_1} \sum_{n_2}\sum_{n_1}\sum_{h_2}\sum_{h_1} \frac{2(l-h_2-h_1)+1}{4\pi} \right.$$
$$\times E^{l,h_2,h_1}_{m,n_2,n_1,n_0}(t) \langle l-h_2,1,n_2,0|l,n_2\rangle \langle l-h_2,1,n_0-j_1,-j_2|l,n_0-j_1-j_2\rangle \langle l-h_2-h_1,1,n_1,0|l-h_2,n_1\rangle$$
$$\left. \times \langle l-h_2-h_1,1,n_0,-j_1|l-h_2,n_0-j_1\rangle - \delta_{j_2,0}\delta_{j_1,0}\delta_{m,n_0} \frac{2l+1}{4\pi}\frac{t^2}{2} e^{-\mu_s t} P^l_{0,0}(\cos\theta) e^{-in_0\phi} \right\}, \quad (24)$$

with

$$E^{l,h_2,h_1}_{m,n_2,n_1,n_0}(t) = \sum_{i,j,f} [B^l_{mn_2}]_i [B^{l-h_2}_{n_2n_1}]_j [B^{l-h_2-h_1}_{n_1n_0}]_f \exp(-\mu_a t)$$
$$\times \left(\frac{\exp(-\lambda_f^{l-h_2-h_1}t) - \exp(-\lambda_i^l t)}{(\lambda_j^{l-h_2} - \lambda_f^{l-h_2-h_1})(\lambda_i^l - \lambda_f^{l-h_2-h_1})} \right.$$
$$\left. - \frac{\exp(-\lambda_j^{l-h_2}t) - \exp(-\lambda_i^l t)}{(\lambda_j^{l-h_2} - \lambda_f^{l-h_2-h_1})(\lambda_i^l - \lambda_j^{l-h_2})} \right), \quad (25)$$

where $i,j,f=1,2,3,4$ for $l \geqslant 2$, and $i,j,f=1,2$ for $l=1,2$.

In SP the component of the unnormalized second moment of $I_m=[I,Q,U,V]$, with the initial polarized state $\mathbf{I}^{SP(0)}$, is obtained by

$$\langle \mathbf{R}_\alpha \mathbf{R}_\beta \rangle^{SP}_m = \sum_{j_1}\sum_{j_2} \frac{1}{2}(U_{\alpha j_1}U_{\beta j_2} + U_{\alpha j_2}U_{\beta j_1})$$
$$\times [\mathbf{T}^{-1}\langle \mathbf{R}_{j_2}\mathbf{R}_{j_1}\rangle \mathbf{T}\mathbf{I}^{SP(0)}]_m. \quad (26)$$

The square of the width of the photon distribution for the linearly polarized component is determined by

$$D_{p,\alpha\beta}(\mathbf{s},t) = \frac{[\langle \mathbf{R}_\alpha\mathbf{R}_\beta\rangle^{SP}_I \pm \langle \mathbf{R}_\alpha\mathbf{R}_\beta\rangle^{SP}_Q]}{2F_\parallel(\mathbf{s},\mathbf{s}_0,t)} - \frac{1}{2}R^c_{p,\alpha}R^c_{p,\beta}, \quad (27)$$

where the + sign holds for the $p=\parallel$ component, and the − sign holds for the $p=\perp$ component. The square of the width of photon distribution for the circularly polarized components is obtained by

$$D_{c,\alpha\beta}(\mathbf{s},t) = \frac{[\langle \mathbf{R}_\alpha\mathbf{R}_\beta\rangle^{SP}_I \pm \langle \mathbf{R}_\alpha\mathbf{R}_\beta\rangle^{SP}_V]}{2F_c(\mathbf{s},\mathbf{s}_0,t)} - \frac{1}{2}R^c_{c,\alpha}R^c_{c,\beta}, \quad (28)$$

where the + sign holds for the $c=R$ component, and the − sign holds for the $c=L$ component.

F. Gaussian distribution of the polarized light

Polarized photon intensity $I_\nu(\mathbf{r},\mathbf{s},t)$, $\nu=\parallel,\perp,R,L$, is expressed by an approximate Gaussian distribution,

$$I_\nu(\mathbf{r},\mathbf{s},t) = \frac{F_\nu(\mathbf{s},\mathbf{s}_0,t)}{(4\pi)^{3/2}} \frac{1}{[\det D_\nu]^{1/2}} \exp\left\{ \sum_{\alpha\beta} -\frac{1}{4}[(D_\nu)^{-1}]_{\alpha\beta} \right.$$
$$\left. \times (r_\alpha - R^c_{\nu,\alpha})(r_\beta - R^c_{\nu,\beta}) \right\}. \quad (29)$$

The ballistic component has been subtracted in the expressions for the angular distribution Eq. (8), for the first cumulant Eq. (19), and for the second cumulant, Eq. (24). This subtraction ensures that the summation over l converges even at very early times, as discussed in Sec. III of Ref. [30].

In the case of the transmission of light, the formalism produces the correct first and second cumulants, but the Gaussian-shaped distribution obtained for early times violates causality, as manifested by the photons at the front edge of the distribution traveling faster than the speed of light in free space. We have introduced an approach to reshape the distribution in Ref. [30], which maintains the correct center position and width of spread of the distribution, and satisfies the causality condition. This technique can be extended to include polarization, combining the formula for the calculation of cumulants of polarized components, in the study of transmission of linear and circular polarized light.

III. RESULT

A. Theoretical result

We now use the formalism developed in Sec. II to study backscattering of circularly polarized light in a scattering medium. A right circularly polarized beam of light with initial Stokes parameters $I=[1,0,0,1]$ and wavelength $\lambda=610$ nm is assumed to be injected into an infinite medium comprised of polystyrene spheres (with refractive index $m=1.59$) suspended in water (with refractive index $m_0=1.33$). The absorption coefficient of light in the medium is assumed to be zero. The light is incident along the z axis from the origin $(x,y,z)=(0,0,0)$. The backscattered light is received by a detector located at $(x_d,0,0)$. Figure 1 shows the computed time-resolved profiles of circularly polarized backscattered light as a function of time t (in a unit of l_{tr}/c), collected at direction $\theta=180°$ and position $x_d=0.5l_{tr}$, where l_{tr} is the transport mean free path, for polystyrene spheres of diameter (a) $d=0.10$ μm, (b) $d=0.213$ μm, (c) $d=0.855$ μm, and (d) $d=8.0$ μm. A remarkable feature is that the backscattered signal is dominated by the left circular polarized (LCP) light if the size of scatterers is small compared to the wavelength of light, as shown in Figs. 1(a) and 1(b), but it is dominated by the right circular polarized (RCP) light if the size of scatterers is large, as displayed in Figs. 1(c) and 1(d). Figure 2 shows how the peak intensity of RCP light and LCP light vary with the size of scatterers.

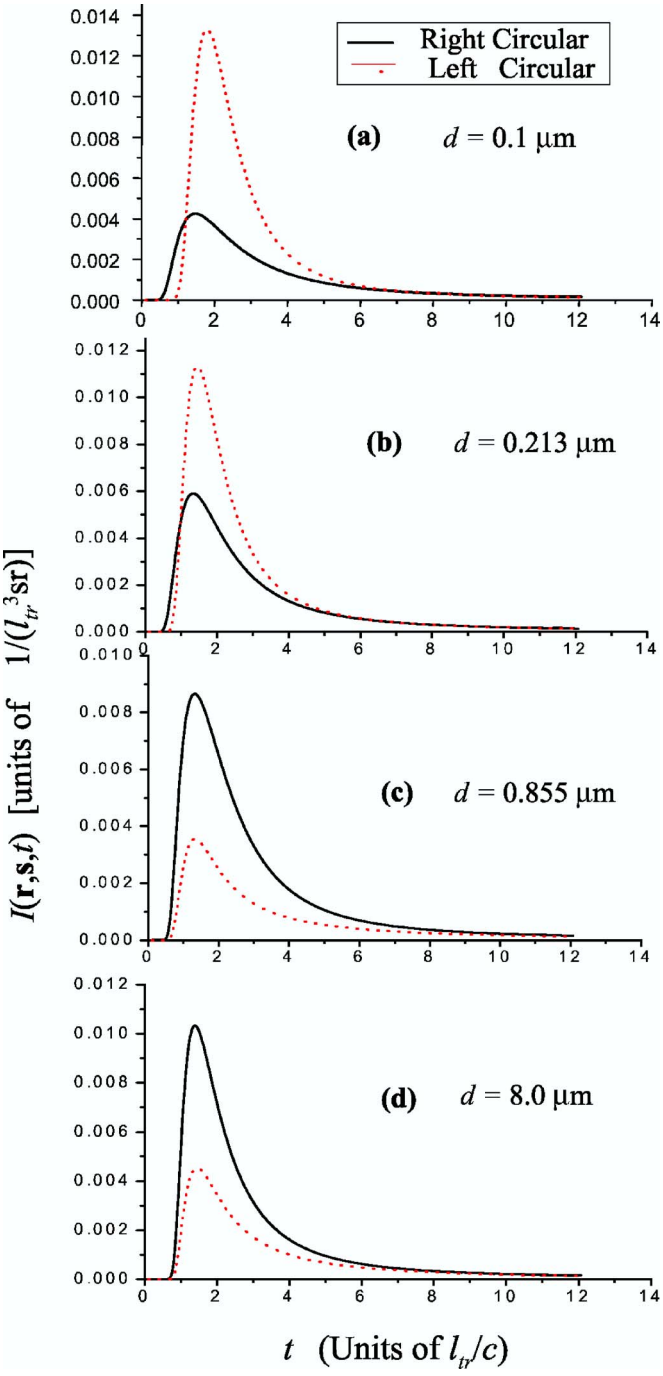

FIG. 1. (Color online) Time-resolved profiles of RCP (solid curve) and LCP (dotted curve) backscattered light intensity as functions of time t (in the unit of l_{tr}/c), received at angle $\theta=180°$ and detector position $x_d=0.5l_{tr}$, where l_{tr} is the transport mean free path, for different diameters of scatterers: (a) $d=0.10$ μm, (b) $d=0.213$ μm, (c) $d=0.855$ μm, and (d) $d=8.0$ μm. The initial Stokes parameters $\mathbf{I}=[1,0,0,1]$ represent a RCP light beam incident along the z direction, and the wavelength $\lambda=610$ nm.

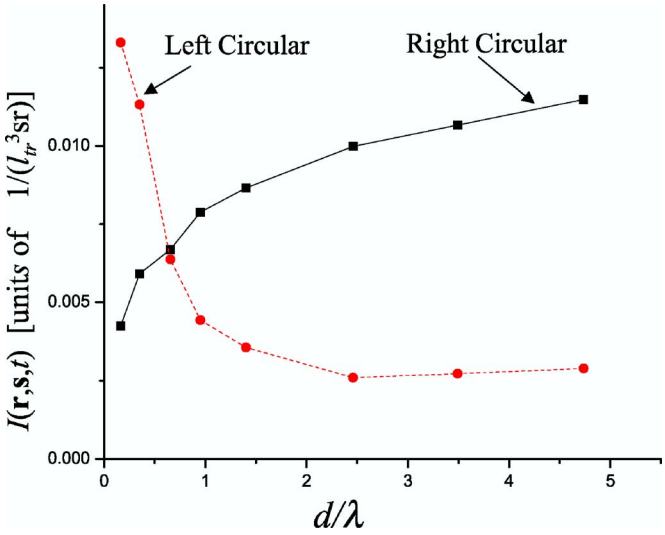

FIG. 2. (Color online) The peak intensity of the time-resolved profile of RCP and LCP backscattered light as functions of d/λ, at angle $\theta=180°$ and detector position $x_d=0.5l_{tr}$. The incident beam is RCP.

We explain this phenomenon by considering the effect of Mie single scattering together with the effect of multiple scattering. The Mie formula indicates that when $m/m_0=1.19$, for small particles the Stokes V component is negative for θ larger than 90°, which means that the helicity of light singly backscattered from a small particle will flip. As the particle size increases, the helicity of the near-backward scattered light computed using Mie formula becomes oscillating, and the region of negative V squeezes to a range near $\theta=180°$. For near-forward scattering, the value of V is positive, hence, the helicity does not flip. For large particles the anisotropy factor g is large, and the probability of near-forward scattering is high. For large particles compared to λ, backscattering results from the accumulated effect of many small-angle (near-forward) scattering events, each of which changes the direction only slightly. These small-angle scattering events do not change the helicity of circularly polarized light. Hence, the backscattered light is dominated by the component that maintains the original helicity. When particles are small, however, the events with large-angle scattering play a more important role. The backscattered light is dominated by the component with the flipped helicity.

In view of the above explanation, it is expected that circularly polarized light with reversed helicity dominates only when the detector is located close to the source. When the distance between the source and the detector becomes large, more backscattered photons come from the accumulation of many small-angle scattering events, and those retain the original helicity. Figure 3 shows the computed time-resolved profiles at different source-detector distances: (a) $x_d=0.1l_{tr}$, (b) $x_d=0.2l_{tr}$, (c) $x_d=1.0l_{tr}$ for a fixed-particle diameter, $d=0.7$ μm, and detection angle $\theta=180°$. We see that the dominant component changes from LCP to RCP as the source-detector distance increases. Figure 4 shows the backscattered time profiles for different detection angles: (a) $\cos\theta=-1$, (b) $\cos\theta=-0.9$, (c) $\cos\theta=-0.8$, for particle diameter $d=0.855$ μm and the source-detector distance $x_d=1.0l_{tr}$. While total intensity increases with a decrease of angle θ, the RCP component remains dominant, which indicates that the helicity of backscattered light is not sensitive to the angle.

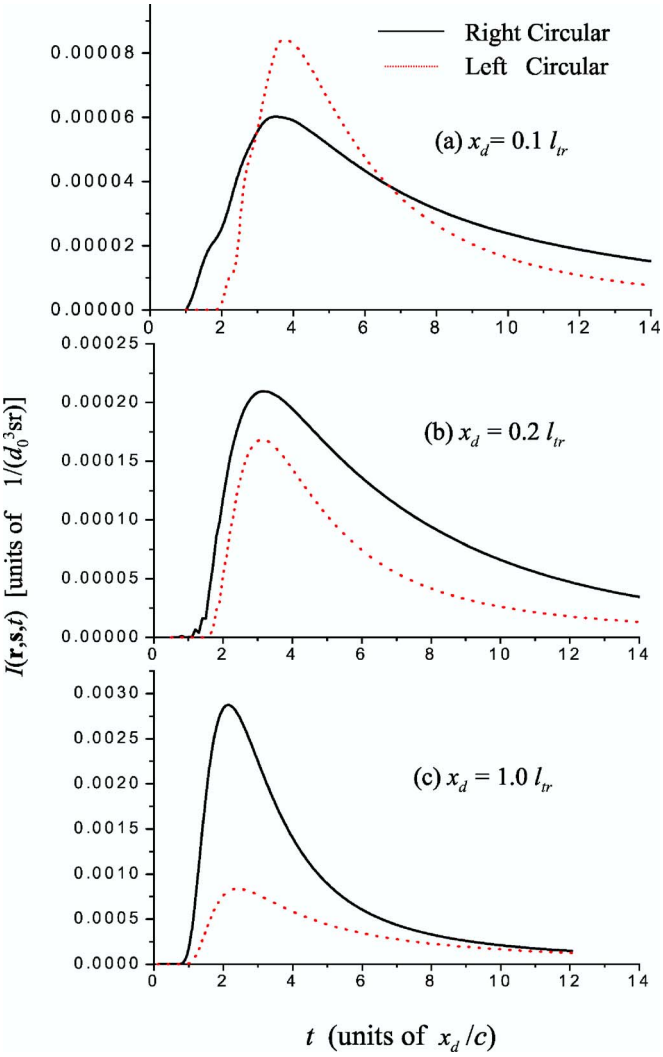

FIG. 3. (Color online) Time-resolved profiles of RCP (solid curve) and LCP (dotted curve) backscattered light as functions of time t, at different source-detector distances: (a) $x_d=0.1l_{tr}$, (b) $x_d=0.2l_{tr}$, (c) $x_d=1.0l_{tr}$, for particle diameter $d=0.7$ μm, the detection angle $\theta=180°$, and the wavelength $\lambda=610$ nm. The incident beam is RCP.

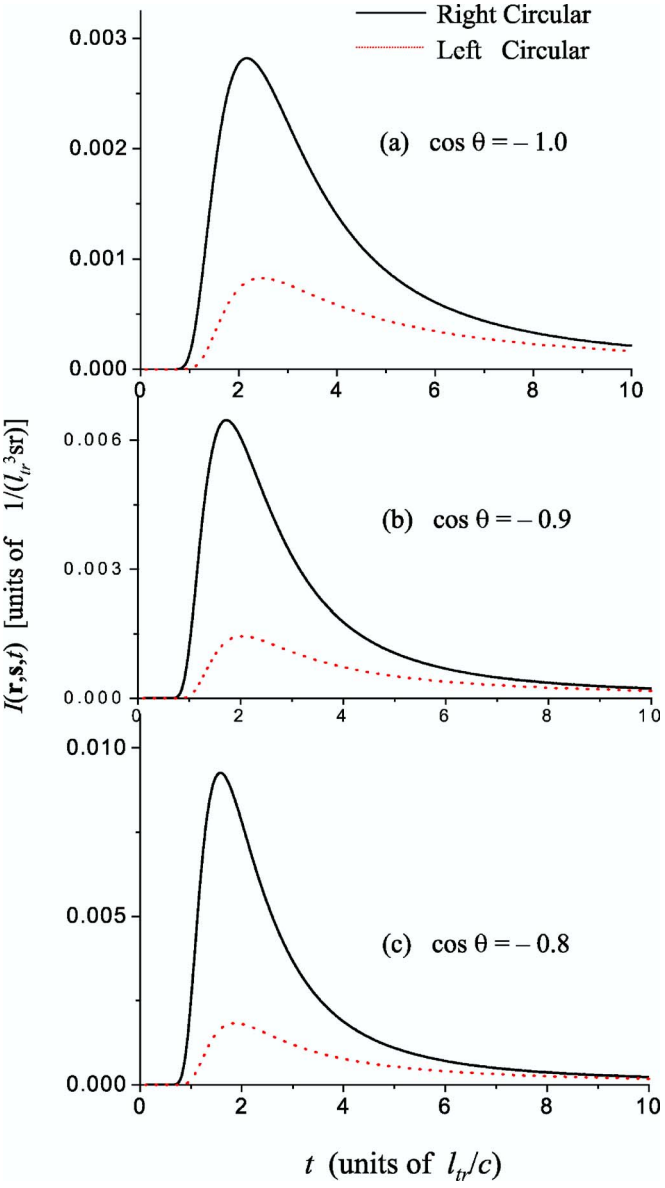

FIG. 4. (Color online) Time-resolved profiles of RCP (solid curve) and LCP (dotted curve) backscattered light as functions of time t, at different angles: (a) $\cos\theta=-1$, (b) $\cos\theta=-0.9$, (c) $\cos\theta=-0.8$, for the particle's diameter $d=0.855$ μm, the detector position $x_d=1.0l_{tr}$, and the wavelength $\lambda=610$ nm. The incident beam is RCP.

B. Comparison with experiments

We compare the above theoretical result with that of our experiments [23]. The setup for the time-resolved backscattering experiment is schematically shown in Fig. 5. The sample comprises polystyrene spheres suspended in deionized water in a $6\times6\times10$ cm^3 glass cell. Ultrashort light pulses of 100 fs duration are generated at a repetition rate of 82 MHZ with wavelength $\lambda=610$ mn by a colliding pulse mode-locked dye laser. A quarter-wave plate is used to obtain RCP light. Time-resolved circularly polarized backscattered light is monitored by a 2 ps resolution streak camera.

Figure 6 shows the time-resolved profiles of backscattered light measured separately, with (a) small particles $d=0.213$ μm ($g=0.389$), scattering coefficients $\mu_s/c=0.61$ cm^{-1} ($l_{tr}=2.68$ cm), and (b) large particles $d=8.0$ μm ($g=0.911$), scattering coefficients $\mu_s/c=0.61$ cm^{-1} ($l_{tr}=18.42$ cm). The detected backscattered light is dominated by the LCP (dotted curve) for small particles in case (a), but it is dominated by the RCP (solid curve) for large particles in case (b), even though the average x_d/l_{tr} for case (b) is much smaller than that for case (a). Figure 7 shows a comparison of normalized circularly polarized intensity of theoretical and experimental results for the case of $d=8.0$ μm ($d/\lambda=13.11$). Considering the differences between the theoretical parameters and the experimental setup (not an infinite medium, uncertainty in source-detector distance) theoretical predictions are in reasonable agreement with the experimental result.

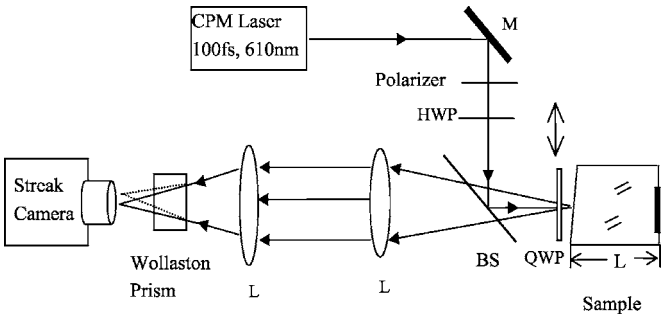

FIG. 5. Schematic diagram of the experimental setup for the time-resolved polarized backscattering measurement (BS=beam splitter, L=lens, M=mirror).

IV. DISCUSSION

A detailed theoretical formalism for the calculation of the distribution of polarized light intensity scattered from an infinite uniform turbid medium has been presented. The formalism is based on an analytical cumulant solution of the vector radiative transfer equation for an arbitrary phase matrix. It is then specialized for a phase matrix obtained from the Mie theory since many practical applications deal with Mie-scattering cases. The scattered polarized photon distribution depends on the size of the scatterers, the distance between the light source and the detector, as well as, on the detection angle.

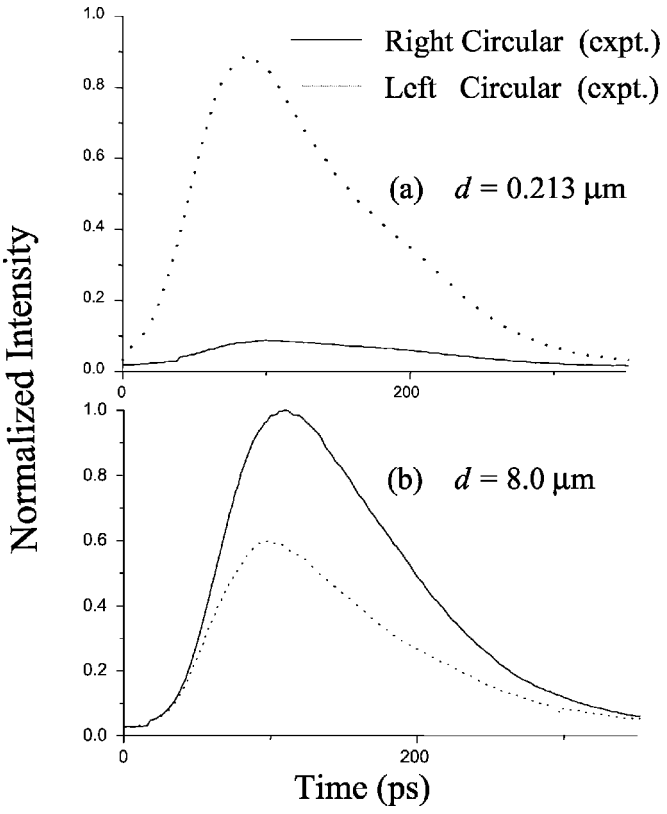

FIG. 6. The experimental time-resolved profiles of RCP (solid curve) and LCP (dotted curve) backscattered light as functions of time t for (a) small particles $d=0.213$ μm ($g=0.389$), the scattering coefficients $\mu_s/c=0.61$ cm^{-1} ($l_{tr}=2.68$ cm), (b) large particles $d=8.0$ μm ($g=0.911$), $\mu_s/c=0.61$ cm^{-1} ($l_{tr}=18.42$ cm). The incident beam is RCP.

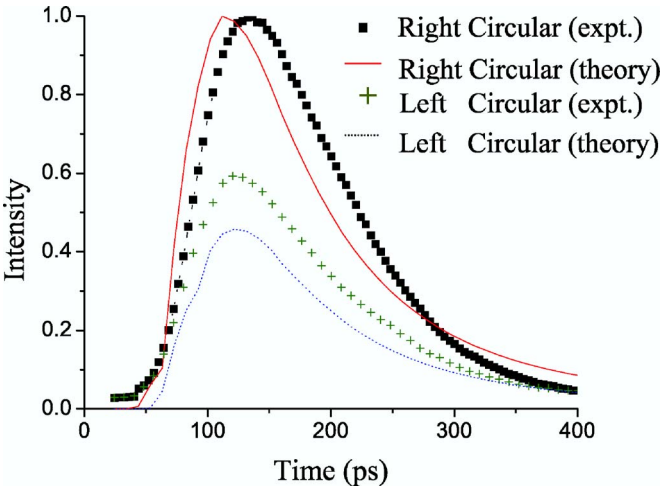

FIG. 7. (Color online) Comparison of theoretical and experimental results of normalized circular polarized light intensity for the medium with a particle diameter $d=8.0$ μm and wavelength $\lambda=610$ nm. The incident beam is RCP.

The advantage of the analytical cumulant solution is that it enables the fast and accurate calculation of the temporal profile of scattered polarized photon distribution. The use of Stoke's representation allows the investigation of light of any polarization state, including linear polarization and circular polarization, which are commonly used in practical applications. We have used a collimated ultrashort input pulse in our formalism, which represents the experimental conditions using picosecond and femtosecond lasers more closely than the plane wave cases used by earlier works [1–6,8,9]. In our formalism, the linear polarization case is handled by setting the initial Stokes vector as [1, 1, 0, 0]. Our initial results for linear polarization are in good agreement with earlier results [4,5].

In this paper, the focus has been on the calculation of circularly polarized light intensity in the backscattering geometry. The formalism enables the calculation of the intensity distribution of multiple backscattered light components that are copolarized and cross polarized with the incident beam for different angles of detection and for different source-detector positions. It is applicable for the analysis of three-dimensional spatially resolved measurements of characteristics of scattering media, such as satellite-based lidar measurements of clouds and aerosols. The approaches using a plane-wave incident beam calculate the backscattered photon flux at the plane of incidence ($z=0$ plane), and simplify the three-dimensional probing problem as a one-dimensional problem [2–6,8,9]. The approaches using Monte Carlo simulation can also handle three-dimensional spatially resolved measurements, but require a long computation time [7,39,40].

Once the copolarized and cross-polarized scattered intensity distributions are calculated, parameters, such as the degree of polarization and image contrast can be readily calculated to take advantage of the polarization memory effect

[25]. One of the results of this work elucidates the dependence of the relative intensities of the backscattered copolarized and cross-polarized light on the size of the scatterers in the turbid medium. We find that when the incident light is right circularly polarized, the backscattered signal is dominated by LCP light if the size of scatterers is smaller than the wavelength of light, but it is dominated by RCP light if the scatterer size is larger than the wavelength of light. The conclusion is in good agreement with our experimental results [23]. The dependence of the helicity of circularly polarized backscattered light on the scatterer size, and the polarization memory effect have been investigated by other authors [6,9,25–27,41]. Mackintosh *et al.* [25] experimentally demonstrated the polarization memory effect for spherical particles suspended and undergoing Brownian motion in a liquid by fitting a simple diffusion-based model to account for temporal correlations of the intensity fluctuations for different polarization channels. The theoretical estimation of backscattering of the circular polarized light using the numerical solution of the VRTE has been performed by Kim and Moscoso [6], as well as Sakami and Dogariu [9], which has been mentioned earlier in the Introduction. Phillips *et al.* [41] used an electric-field Monte Carlo method to study the backscattering of circularly polarized beams normally incident on a half space of scattering particles and found that the backscattered light of the same helicity formed a ring centered on the point of incidence. A Monte Carlo approach has been used by other researchers as well [7,39,40]. Xu and Alfano [27] used a random-walk approach to analytically estimate the characteristic depolarization length, which is obtained as an average over the entire detection solid angle. All these approaches converge on the general result that the circularly polarized light of the same helicity dominates backscattering when the scatterer size is larger than the light wavelength, as does the formalism presented in this paper and experimental results [23]. The salient feature of this work is that it provides an analytical approach for the calculation of polarized scattered light intensity, an experimentally measurable quantity, as a function of time, detection angle, and source-detector separation.

The dependence of the polarized backscattered light on the size of the scatterers in the medium has many potential applications, including biomedical imaging [13–15], flow cytometry [18,19], investigation of biological cell differentiation [17,18], subsurface imaging of cracks and corrosion below paint layers [42,43], lidar-based remote sensing of investigation of cloud and aerosol distribution in atmosphere [20,21], and the imaging of targets in turbid water [22].

Biomedical and biophysical applications represent an increasingly important area of application of polarized light scattering. As early as 1976, polarized light scattering was identified as a "new biophysical tool" [6]. The scatterers in biological materials include cells, cell nuclei, mitochondria that are in the Mie scattering domain (typical size varies from 5–20 μm as compared to the wavelength of light in the visible to NIR of 0.5–1.5 μm). Polarization effects in scattered light have been used to study bacterial suspensions in water [16,19], distinguish between a number of leukocyte types in flow cytometry [44,18], cell differentiation [17], and polynucleosome superstructures [45]. It has recently been shown experimentally that backscattered light may be analyzed to obtain information about the size distribution of the cell nuclei [15,46], which in turn could be useful for cancer detection as the cell nucleus size, shape, and distribution changes with cancer progression. In biomedical imaging applications polarization effects in scattering have been shown to be useful in examining skin [47], and subsurface structures in the prostate and other tissues [48].

Another important area of application of polarized light scattering is the remote sensing of the atmosphere and earth. Radar technology, the workhorse for remote sensing of the earth and the atmosphere, makes use of radio waves and its depolarization to obtain information about remote targets and ground flora [49]. While single-scattering approximation of radio waves is reasonable for radar applications [1], for probing of dense cloud, fog, and aerosols in the atmosphere, multiple scattering of light needs to be considered, which the formalism developed in this article does. Different scatterers in the atmosphere have varied size distributions [1,50], such as cloud and fog droplets (radii generally <100 μm, mean radii typically 2.5–5 μm), aerosols (typically <1 μm), and hydrometeors (typically 1 μm or higher). Lidar-based investigation of cloud, aerosols, and other atmospheric scatterers employ visible and near-infrared light (typically 532 nm and 1064 nm) [20,51]. Scatterer size to wavelength ratio the dictates the use of Mie theory for the study of light scattering by clouds and aerosols. In the CALIPSO (Cloud-Aerosol Lidar and Infrared Pathfinder Satellite Observations) mission of NASA [51] one of the tasks involves probing with linearly polarized 532 nm and 1064 nm nanosecond duration pulses and the analysis of the temporal profiles of backscattered light for assessing the vertical distribution of clouds and aerosols in the atmosphere. Pal and Carswell [21] have observed spatial variations in the polarization properties of multiple-scattered light backscattered from clouds. Clearly these types of experimental data and those obtained by extending measurements to even shorter pulses and circularly polarized beams are fertile grounds for the application of the formalism presented in this paper.

ACKNOWLEDGMENTS

This work was supported in part by NASA URC—Center for Optical Sensing and Imaging at CCNY (NASA Grant No. NCC-1-03009), by the Office of Naval Research (ONR), and in part by U.S. Army Medical Research and Materials Command.

APPENDIX: CLEBSCH-GORDAN COEFFICIENTS AND *d*-FUNCTION

For the convenience of the reader, we list the formula of angular momentum we used in this paper.

The following formula for Clebsch-Goldan coefficients $\langle l-h,1,m,-j|l,m-j\rangle$ are useful for our calculation,

$$\langle l-h,1,m,-j|l,m-j\rangle = \begin{Bmatrix} \left[\frac{(l-m)(l-m+1)}{2l(2l-1)}\right]^{1/2} & \left[\frac{(l+m)(l-m+1)}{2l(l+1)}\right]^{1/2} & \left[\frac{(l+m)(l+m+1)}{(2l+2)(2l+3)}\right]^{1/2} \\ \left[\frac{(l-m)(l+m)}{l(2l-1)}\right]^{1/2} & \frac{m}{[l(l+1)]^{1/2}} & -\left[\frac{(l+m+1)(l-m+1)}{(l+1)(2l+3)}\right]^{1/2} \\ \left[\frac{(l+m)(l+m+1)}{2l(2l-1)}\right]^{1/2} & -\left[\frac{(l-m)(l+m+1)}{2l(l+1)}\right]^{1/2} & \left[\frac{(l-m)(l-m+1)}{(2l+2)(2l+3)}\right]^{1/2} \end{Bmatrix}, \quad (30)$$

where the row index (from above) $j=1,0,-1$ and the column index (from left) $h=1,0,-1$.

For obtaining $d^l_{mn}(x)$, the following recurrence relation is used:

$$d^l_{mn}(x) = \frac{1}{(l-1)[(l^2-m^2)(l^2-n^2)]^{1/2}} \times \{(2l-1)[l(l-1)x-mn]d^{l-1}_{mn}(x) - l\{[(l-1)^2-m^2][(l-1)^2-n^2]\}^{1/2}d^{l-2}_{mn}(x)\}, \quad (31)$$

for $l>\max(|m|,|n|)$, with

$$d^{\max(|m|,|n|)}_{mn}(x) = \frac{1}{2^{\max(|m|,|n|)}}\left[\frac{[2\max(|m|,|n|)]!}{(|m-n|)!(|m+n|)!}\right]^{1/2} \times (1-x)^{|m-n|/2}(1+x)^{|m+n|/2}, \quad (32)$$

and $d^l_{mn}(x)=0$ for $l<\max(|m|,|n|)$. For $m=0$, $n=0$ we have $d^0_{00}(x)=1$, $d^1_{00}(x)=x$, and

$$ld^l_{00}(x) = (2l-1)xd^{l-1}_{00}(x) - (l-1)d^{l-2}_{00}(x). \quad (33)$$

[1] A. Ishimaru, *Wave Propagation and Scattering in Random Media* (Institute of Electrical and Electronic Engineers, New York, 1997).
[2] R. L. T. Cheung and A. Ishimaru, Appl. Opt. **21**, 3792 (1982).
[3] Q. Ma, A. Ishimaru, and Y. Kuga, Radio Sci. **25**, 419 (1990).
[4] A. Ishimaru, S. Jaruwatanadilok, and Y. Kuga, Appl. Opt. **40**, 5495 (2001).
[5] A. D. Kim and M. Moscoso, Phys. Rev. E **64**, 026612 (2001); SIAM J. Comput. **23**, 2075 (2002).
[6] A. D. Kim and M. Moscoso, Opt. Lett. **27**, 1589 (2002).
[7] R. Vaillon, B. T. Wong, and M. P. Mengüc, J. Quant. Spectrosc. Radiat. Transf. **84**, 383 (2004).
[8] Y. Jiang, Y. L. Yung, S. P. Sander, and L. D. Travis, J. Quant. Spectrosc. Radiat. Transf. **84**, 169 (2004).
[9] M. Sakami and A. Dogariu, J. Opt. Soc. Am. A **23**, 664 (2006).
[10] A. A. Kokhanovsky, *Light Scattering Media Optics: Problems and Solutions*, 3rd ed. (Springer and Praxis Publishing, Chichester, 2004).
[11] D. Bicout, C. Brosseau, A. S. Martinez, and J. M. Scdhmitt, Phys. Rev. E **49**, 1767 (1994).
[12] R. Carminati, R. Elaloufi, and J. J. Greffet, Phys. Rev. Lett. **92**, 213903 (2004).
[13] A. H. Hielscher, J. R. Mourant, and I. Bigio, Appl. Opt. **36**, 125 (1997).
[14] S. G. Demos and R. R. Alfano, Appl. Opt. **36**, 150 (1997).
[15] V. Backman, R. Gurjar, K. Badizadegan, I. Itzkan, R. R. Dasari, L. T. Perelman, and M. S. Feld, IEEE J. Sel. Top. Quantum Electron. **5**, 1019 (1999).
[16] W. S. Bickel, J. F. Davidson, D. R. Huffman, and R. Kilkson, Proc. Natl. Acad. Sci. U.S.A. **73**, 486 (1976).
[17] W. S. Bickel and M. E. Stafford, J. Biol. Phys. **9**, 53 (1981).
[18] B. G. deGrooth, L. W. M. M. Terstappen, G. J. Puppels, and J. Greve, Cytometry **8**, 539 (1987).
[19] B. V. Bronk, W. P. van de Merwe, and M. Stanley, Cytometry **13**, 155 (1992).
[20] D. M. Winker, W. H. Hunt, and C. A. Hostetler, *Proceedings of Laser Radar Techniques for Atmospheric Sensing*, edited by U. N. Singh [Proceedings of SPIE **5575**, 8 (2004)].
[21] S. R. Pal and A. I. Carswell, Appl. Opt. **24**, 3464 (1985).
[22] G. W. Kattawar and M. J. Rakovic, Appl. Opt. **38**, 6431 (1999).
[23] X. Ni and R. R. Alfano, Opt. Lett. **29**, 2773 (2004).
[24] G. D. Lewis, D. L. Jordan, and P. J. Roberts, Appl. Opt. **38**, 3937 (1999).
[25] F. C. MacKintosh, J. X. Zhu, D. J. Pine, and D. A. Weitz, Phys. Rev. B **40**, 9342 (1989).
[26] F. C. MacKintosh and S. John, Phys. Rev. B **40**, 2383 (1989).
[27] M. Xu and R. R. Alfano, Phys. Rev. Lett. **95**, 213901 (2005); Phys. Rev. E **72**, 065601 (2005).
[28] W. Cai, M. Lax, and R. R. Alfano, Phys. Rev. E **61**, 3871 (2000).
[29] W. Cai, M. Lax, and R. R. Alfano, J. Phys. Chem. B **104**, 3996 (2000).
[30] W. Cai, M. Xu, and R. R. Alfano, Phys. Rev. E **71**, 041202 (2005).
[31] W. Cai, M. Lax, and R. R. Alfano, Phys. Rev. E **63**, 016606 (2000).
[32] M. Born and E. Wolf, *Principles of Optics*, 7th ed. (Cambridge University Press, Cambridge, England, 2002).

[33] S. Chandrasekhar, *Radiative Transfer* (Clarendon, Oxford, 1950).
[34] I. Kuščer and M. Ribarič, Opt. Acta **6**, 42 (1959).
[35] J. W. Hovenier and C. V. M. van der Mee, Astron. Astrophys. **128**, 1 (1983).
[36] B. M. Brink and G. M. Satchler, *Angular Momentum* (Clarendon Press, Oxford, 1962).
[37] M. I. Mishchenko, L. D. Travis, and A. A. Lacis, *Scattering, Absorption, and Emission of Light by Small Particles* (Cambridge University Press, Cambridge, 2002).
[38] R. P. Feyman, Phys. Rev. **84**, 108 (1951).
[39] M. J. Rakovic, G. W. Kattawar, M. Mehrubeoglu, B. D. Cameron, L. V. Wang, S. Rastegar, and G. L. Cote, Appl. Opt. **38**, 3399 (1999).
[40] S. Bartel and A. H. Hielscher, Appl. Opt. **39**, 1580 (2000).
[41] K. G. Phillips, M. Xu, S. K. Gayen, and R. R. Alfano, Opt. Express **13**, 7954 (2005).
[42] J. H. Ali, W. B. Wang, P. P. Ho, and R. R. Alfano, Opt. Lett. **25**, 1303 (2000).
[43] J. H. Ali, W. B. Wang, R. R. Alfano, and M. K. Kassir, Theor. Appl. Fract. Mech. **41**, 1 (2000).
[44] G. C. Salzman, S. B. Singham, R. G. Johnston, and C. F. Bohren, in *Flow Cytometry and Sorting*, 2nd ed. (Wiley-Liss, New York, 1990).
[45] S. Zeitz, A. Belmont, and Nicolini, Cell Biophys. **5**, 163 (1983).
[46] L. T. Perelman, V. Backman, M. Wallace, G. Zonois, R. Manoharan, A. Nusrat, S. Shields, M. Seiler, T. Hamano, I. Itzkan, J. van Dam, J. M. Crawford, and M. S. Feld, Phys. Rev. Lett. **80**, 627 (1998).
[47] R. R. Anderson, Arch. Dermatol. **127**, 1000 (1991).
[48] W. B. Wang, J. H. Ali, R. R. Alfano, J. H. Vitenson, and J. M. Lombardo, IEEE J. Sel. Top. Quantum Electron. **9**, 228 (2003).
[49] M. I. Skolnik, *Introduction to Radar Systems* (McGraw-Hill, New York, 1962).
[50] V. E. Zuev, A. A. Zemlyanov, Y. D. Kopytin, and A. V. Kuzikovskii, *High-Power Laser Radiation in Atmospheric Aerosols* (D. Reidel Publishing, Dordrecht, 1984).
[51] D. M. Winker, J. R. Pelon, and M. P. McCormick, *Proceedings of the Conference of Lidar Remote Sensing for Industry and Environment Monitoring III*, edited by U. N. Singh, T. Itabe, and Z. Liu [Proceedings of SPIE **4893**, 1 (2003)].